

Article

# Fabrication of Silver- and Zinc-Doped Hydroxyapatite Coatings for Enhancing Antimicrobial Effect

Daniela Predoi <sup>1</sup>, Simona Liliana Iconaru <sup>1</sup> and Mihai Valentin Predoi <sup>2,\*</sup>

<sup>1</sup> National Institute of Materials Physics, Atomistilor Street, No. 405A, P.O. Box MG 07, 077125 Magurele, Romania; dpredoi@gmail.com (D.P.); simonaiconaru@gmail.com (S.L.I.)

<sup>2</sup> Department of Mechanics, University Politehnica of Bucharest, BN 002, 313 Splaiul Independentei, Sector 6, 060042 Bucharest, Romania

\* Correspondence: predoi@gmail.com or mihai.predoi@upb.ro

Received: 23 August 2020; Accepted: 18 September 2020; Published: 20 September 2020



**Abstract:** This study develops, for the first time, composite coatings based on silver and zinc doped hydroxyapatite in chitosan matrix (AgZnHApCs). The AgZnHApCs composite coatings were prepared by dip coating method. The hydroxyapatite (HAp), biocompatible material for regenerating and strengthening damaged bones were doped with silver and zinc ions and coated with chitosan in order to produce a uniform and homogenous coating with biocompatibility and antimicrobial properties. The stability of AgZnHApCs suspensions was evaluated by ultrasound measurements. The value of stability parameters of AgZnHApCs suspension is in good agreement with the value of bidistilled water used as reference fluid. Homogeneously dispersed solutions of AgZnHApCs were synthesized to endeavor to optimize the physico-chemical and biological characteristics of the coatings obtained at room temperature. The AgZnHApCs composite suspension and coatings were analyzed using various investigation techniques, such as X-ray diffraction (XRD), Fourier transformed infrared spectroscopy (FTIR), MTT (3-[4,5-dimethylthiazol-2-yl]-2,5-diphenylte-2H-tetrazolium bromide) assay and antimicrobial studies. The optical spectroscopy, atomic force microscopy (AFM), metallographic examination and X-ray photoelectron spectroscopy (XPS) on AgZnHApCs composite coatings were also conducted. Cell culture and MTT assays demonstrate that AgZnHApCs composite suspension and coatings have no negative effect on the cell viability and proliferation. The cell morphology was not affected in presence of AgZnHApCs composite suspension and coatings. The antimicrobial assays conducted against *Staphylococcus aureus* ATCC 25923, *Escherichia coli* ATCC 25922, and *Candida albicans* ATCC 90029 microbial strains revealed that both the AgZnHApCs composite suspension and coatings exhibited great antimicrobial properties.

**Keywords:** hydroxyapatite; composite coatings; silver; zinc; chitosan; antimicrobial activity

## 1. Introduction

The development of new materials with enhanced antimicrobial properties is one of the priority research areas in the last years. An important property of these materials is represented by the possibility of their use in the biomedical field [1]. Several studies reported in the literature have shown on the one hand that the occurrence of infections leads to a significant increase in medication costs (hospitalization), and on the other hand, it has been shown that the use of antibiotics before surgery does not bring real benefit to patients; they can even lead (when misused) to the appearance of antibiotic-resistant bacteria, these infections being much more difficult to treat [2]. One of the most studied materials with application in various domain such as dentistry and implantology is hydroxyapatite (HAp,  $\text{Ca}_{10}(\text{PO}_4)_6(\text{OH})_2$ , Ca/P ratio of 1.67) [1,3].

HAp is the major inorganic component of bone tissue and has a structure with a special affinity that allows it to be substituted with various ions, such as: Zinc ( $Zn^{2+}$ ), Magnesium ( $Mg^{2+}$ ), Silver ( $Ag^+$ ), carbonate ( $CO_3^{2-}$ ), etc. [2]. Therefore, once a substitution occurs, there is a significant change in the physicochemical and biological properties of hydroxyapatite [4]. This behavior allows one to improve the properties of HAp, including antibacterial ones, through substitutions [4–8]. Among the properties of synthetic HAp we mention: excellent biocompatibility, good bioactivity, osteoconductivity, chemical and crystallographic similarity with natural hydroxyapatite [1]. Due to the fact that hydroxyapatite does not have antimicrobial properties, and yet it is used in various biomedical applications, one way to improve these properties is to dope HAp with antimicrobial agents. Therefore, to make it suitable to fight with antibiotic resistant bacteria, we chose to dope HAp with  $Ag^+$  and  $Zn^{2+}$  ions. Materials based on HAp doped with Ag and/or zinc ions can be obtained by several methods, among which we mention: hydrothermal method [2], microwave [9] wet-chemical method [1], sol-gel process [10,11], co-precipitation [12–14], chemical solution deposition [5], etc.

Silver is one of the most used and studied antimicrobial agents due to its broad spectrum of action and low toxicity at low concentrations [15,16]. Compared to Silver, Zinc is a chemical element that is found naturally in bone tissue and is essential for biological processes such as: enzyme activity, DNA synthesis, mitosis, cell proliferation, etc. [5,9]. Recently, in their study, van Hengel et al. [4] have shown that surfaces functionalized with zinc and silver ions exhibit antimicrobial activity, even against bacterial strains of methicillin-resistant *Staphylococcus aureus* (MRSA). The use of metallic ions (Silver and Zinc) as antimicrobial agents give to hydroxyapatite the ability to fight against gram-positive (*Staphylococcus aureus*, *Streptococcus mutans*, *Bacillus cereus*) [1,7,17,18], gram-negative (*Escherichia coli*, *Aggregatibacter actinomycetemcomitans*, *Fusobacterium nucleatum*) [7,10] bacterial strains and fungi (*Candida albicans*) [1].

On the other hand, studies reported in the literature have shown that the antimicrobial properties of compounds based on hydroxyapatite doped with silver or zinc ions are strongly dependent on the concentration of antimicrobial agent in the samples [8,13]. Taking into account the aspects mentioned above, the mechanism of antimicrobial action of both Ag and Zn compounds are not yet fully understood [1,19]. Furthermore, a widely used material due to its remarkable biodegradability and biocompatibility in recent years, mostly in dental applications, is chitosan. Chitosan is a biopolymer isolated from shellfish, crab and shrimp which was reported as having antimicrobial properties and antioxidant activity [20–22].

The aim of this study was to develop a novel AgZnHApCs composite with superior biocompatibility and significant antibacterial activity. A mixture suspension of silver and zinc doped hydroxyapatite and chitosan with a good stability was analyzed by ultrasound measurement and XRD, FTIR, MTT and antimicrobial activity in order to be used in obtaining uniform and homogeneous coatings that preserve the biological properties of the suspension. The novel AgZnHApCs composite coatings obtained were evaluated by XRD, FTIR, optical spectroscopy, atomic force microscopy (AFM), metallographic examination, XPS, MTT and antimicrobial activity.

## 2. Materials and Methods

### 2.1. Materials

The reagents used in the synthesis of the materials such as chitosan (Cs) powder (low molecular weight, 75–85% deacetylated), calcium nitrate tetrahydrate, zinc nitrate hexahydrate, silver nitrate, ammonium hydrogen phosphate, ethanol absolute and acetic acid were purchased from Sigma Aldrich, St. Louis, MO, USA, and all were of analytical grade. The double distilled water and deionized water were also used in the experiment.

## 2.2. Silver and Zinc Doped Hydroxyapatite in Chitosan Matrix (AgZnHApCs)

The synthesis of silver- and zinc-doped hydroxyapatite in chitosan matrix with  $x_{\text{Ag}} = 0.1$  and  $x_{\text{Zn}} = 0.1$  was effectuated using an adapted coprecipitation method [23] with  $(\text{Ca} + \text{Ag} + \text{Zn})/\text{P}$  was fixed to 1.67 [24,25]. In the first step, 0.1 g of chitosan (Cs) was added to 100 mL deionized water containing 1% and stirred until a clear solution is obtained (about 2 h). In the second step,  $(\text{NH}_4)_2\text{HPO}_4$  was dissolved in 50 mL ethanol and added in 100 mL chitosan solution and stirred for 2 h at 40 °C. At the same time,  $\text{Ca}(\text{NO}_3)_2 \cdot 4\text{H}_2\text{O}$ ,  $(\text{AgNO}_3)$  and  $\text{Zn}(\text{NO}_3)_2 \cdot 6\text{H}_2\text{O}$  were dissolved in ethanol and mixed for 2 h at 40 °C. The solution containing Ca, Ag and Zn was added dropwise in the solution containing P and Cs. The final solution was stirred for 2 h at 100 °C. The resulting solution of AgZnHApCs was centrifuged and redispersed in solution of chitosan and stirred at room temperature for 4 h. The resulting suspension was analyzed from a stability point of view and used to prepare the coatings.

## 2.3. Preparation of AgZnHApCs Coatings

The AgZnHApCs coatings were obtained using a dip coating method which was previously described in [26]. AgZnHApCs coatings were deposited on the glass substrate. The obtained AgZnHApCs layer was dried at 100 °C for 24 h.

## 2.4. Characterization Methods

Ultrasonic measurements were performed on 100 mL of concentrated suspension of 5Sm-HAp [6,27,28]. The digitalized ultrasonic signals were recorded on the digital oscilloscope at a very precise interval of 5.00 s. In order to have an accurate evaluation of the stability of the 5Sm-HAp suspension, the double distilled water (the most stable suspension) was chosen as the reference fluid, under the same experimental conditions.

The synthesized silver and zinc doped hydroxyapatite in chitosan matrix were characterized by X-ray diffraction (XRD, Bruker D8 Advance diffractometer, Bruker, Billerica, MA, USA,  $\text{CuK}\alpha$  radiation) technique in the range of  $2\theta$  values from 10–60° at a step of 0.02° and 34 s measuring time per step.

The molecular structure of the samples was also studied by FTIR-ATR spectroscopy in the 400–4000  $\text{cm}^{-1}$  spectral range using a Perkin Elmer instrument (Waltham, MS, USA).

The X-ray photoelectron spectroscopy measurements (XPS) were recorded with a multimethod SPECS surface analysis system, as previously described in [29,30].

Furthermore, the surface morphology of the coatings was investigated by atomic force microscopy (AFM) with the aid of an NT-MDT NTEGRA Probe Nano Laboratory instrument (NT-MDT, Moscow, Russia), as previously reported in [31]. The data analysis of the 2D surface topographies, as well as the 3D representation of the AFM images, were performed with the aid of Gwyddion 2.55 software [32].

In addition, the morphology of the surface coatings was studied by optical and metallographic microscopy as previously described in [33]. The image processing of the recorded data was performed using Image J software (ImageJ 1.51j8, National Institutes of Health, Bethesda, MD, USA) [32].

The cytotoxicity of the AgZnHApCs suspensions and coatings was assessed by MTT (3-(4,5-dimethylthiazol 2,5-diphenyltetrazolium bromide) assay, in agreement with previous studies [34]. For this purpose, human fetal osteoblasts (hFOB 1.19) from the American Type Culture Collection (ATCC) were used. The cells were grown in Dulbecco's modified Eagle's medium (DMEM), enriched using L-glutamine (2.5 mM), sodium pyruvate (0.5 mM), non-essential amino acids (0.1 mM), baking soda (1.2 g/L) and fetal bovine serum. Afterwards, the cultures were incubated in the atmosphere with 5%  $\text{CO}_2$  at 37 °C. All subsequent passages were performed at confluence (approximately  $2 \times 10^6$  cells/plate), on average at 5–6 days, the ratio being 1/3. After that, the cells were seeded in a Petri dish, including in the control sample (Petri dish without sample), at a concentration of  $3 \times 10^6$  cells/flask of 75  $\text{cm}^2$ . The cultures were incubated with the samples in the atmosphere with 5%  $\text{CO}_2$ , at 37 °C, and after 1, 7 and 14 days, the cells are visualized under an inverted microscope and pictures were taken in the visible (VIS) with a digital camera. For the quantitative cytotoxic assay, the cells were treated with MTT solution [3-(4,5-dimethylthiazoly)-2,5-diphenyltetrazolium bromide]

and incubate in an atmosphere with 5% CO<sub>2</sub> at 37 °C and the optical density of formazane solubilized at 595 nm using a TECAN spectrophotometer (Tecan GENios, Grödic, Germany) was quantified in order to obtain the cell viability of the cells. The experiments were performed 4 times and the data were presented as mean ± SD.

The antimicrobial properties of the AgZnHAp suspensions and coatings were studied against reference microbial strains *Staphylococcus aureus* ATCC 25923, *Escherichia coli* ATCC 25922, and *Candida albicans* ATCC 90029. The antimicrobial assays were performed by preparing 0.5 McFarland standard microbial cultures, as previously described in [35]. Afterwards, the AgZnHApCs suspensions and coatings were exposed to 2 mL of microbial suspension of 5 × 10<sup>6</sup> CFU/mL (colony forming units/mL) in phosphate-buffered saline (PBS) in a Petri dish and incubated for 24, 48 and 72 h. As a positive control, a free microbial culture was assessed at the same time intervals. Afterwards, the suspension was collected at different time intervals (24, 48 and 72 h) and incubated on LB agar medium for 24 h at 37 °C. The number of CFU/mL was determined for each of the incubated samples with the microbial suspensions. The experiments were performed 4 times and the data were presented as mean ± SD. Statistical analysis was done using the ANOVA single factor test.

### 3. Results

The stability of AgZnHApCs suspension was evaluated by ultrasonic measurements performed on 100 mL suspension. Ultrasonic waves propagate in liquids and di-phasic systems (e.g., suspensions), bringing information about the medium in which these waves propagate. One advantage of this method, compared to optical methods, is the possibility of characterizing opaque fluids. The frequencies which are currently used are between 1 MHz and 50 MHz. The digitalized ultrasonic signals were recorded using two pairs of coaxial ultrasonic transducers; one pair with a central frequency of 5 MHz and the other pair with a central frequency of 25 MHz. The interval at which the ultrasonic signals were recorded was 5.00 s. We consider a suspension to be stable if the amplitude of the overall signal has a weak change of amplitude during the monitored sedimentation process. Of course, in pure water, our reference is perfectly stable (zero variation of ultrasonic echo amplitude). We determine the slope of the amplitude during the monitoring period, to determine a quantitative stability parameter, defined in the manuscript. A short echo comprises several superposed signals of different frequencies, as the Fourier series can provide. We determine the variation of amplitudes for a number of frequencies also, during the monitoring period. The evolution of the signals in time gives us important information about the stability of the suspension and the attenuation vs. time. The value of the stability parameter  $s = \frac{1}{A_m} \left| \frac{dA}{dt} \right|$  calculated for the AgZnHApCs suspension had the value 1.77 × 10<sup>-5</sup> s<sup>-1</sup> using a pair of coaxial ultrasonic transducers, both of central frequency of 5 MHz and 6.2 × 10<sup>-7</sup> s<sup>-1</sup> using a pair of coaxial ultrasonic transducers, both of central frequency of 25 MHz. The values obtained for the stability parameter indicated a very good stability. Another characteristic regarding the stability of AgZnHApCs suspension is the frequency spectrum of the first transmitted echo (Figure 1). Using transducers of 5 MHz central frequency, the peaks of amplitudes at 4 MHz, for the reference fluid, are also peaks for the measured signals. More relevant information is represented by the spectral amplitudes' variation during the experiment (Figure 1a). From the Fourier spectrum, were selected frequencies 2–8 MHz (Figure 1a). On (Figure 1b) is presented the frequency spectrum for the 10–40 MHz range using transducers of 25 MHz central frequency. The behavior of the measured signals is similar to that of the reference fluid. The peaks of amplitudes at 11.5 and 23 MHz, for the reference fluid, are also peaks for the measured signals (Figure 1b). For AgZnHApCs suspension, the typical decreasing values with increasing frequency components were obtained (Figure 2). Based on the 30 mm distance between the coaxial transducers, the attenuation vs. frequency in nepper/m can be obtained, averaged over the 5000 s recording period (Figure 2). Compared to distilled water, the ultrasonic signals attenuation is larger in the tested AgZnHApCs suspension. The ultrasonic signals attenuation has classical, continuously increasing values vs. frequency, over the selected frequency range. The experiments were resumed using a pair of coaxial transducers of 25 MHz central frequency. The most relevant

supplementary information was presented in Figure 2b. In intervals of 10–25 MHz, the absorbed energy translates into signal attenuation, visible in the local peak at 20 MHz (Figure 2b). The other peak at 30 MHz, is obtained in a frequency interval of weak signals, and has to be verified in future experiments centered at these higher frequencies. In the range of 25–40 MHz, the behavior of attenuation vs. frequency for the first transmitted echo at 25 MHz central frequency for the AgZnHApCs suspension has a behavior similar to that of bi-distilled water as a reference fluid (Figure 2b). Based on the results obtained, we can say that the suspension is very stable. The information brought by analyzing the first transmitted echo provides relevant information for a characterization from the ultrasonic point of view, in terms of stability, overall and spectral attenuation.

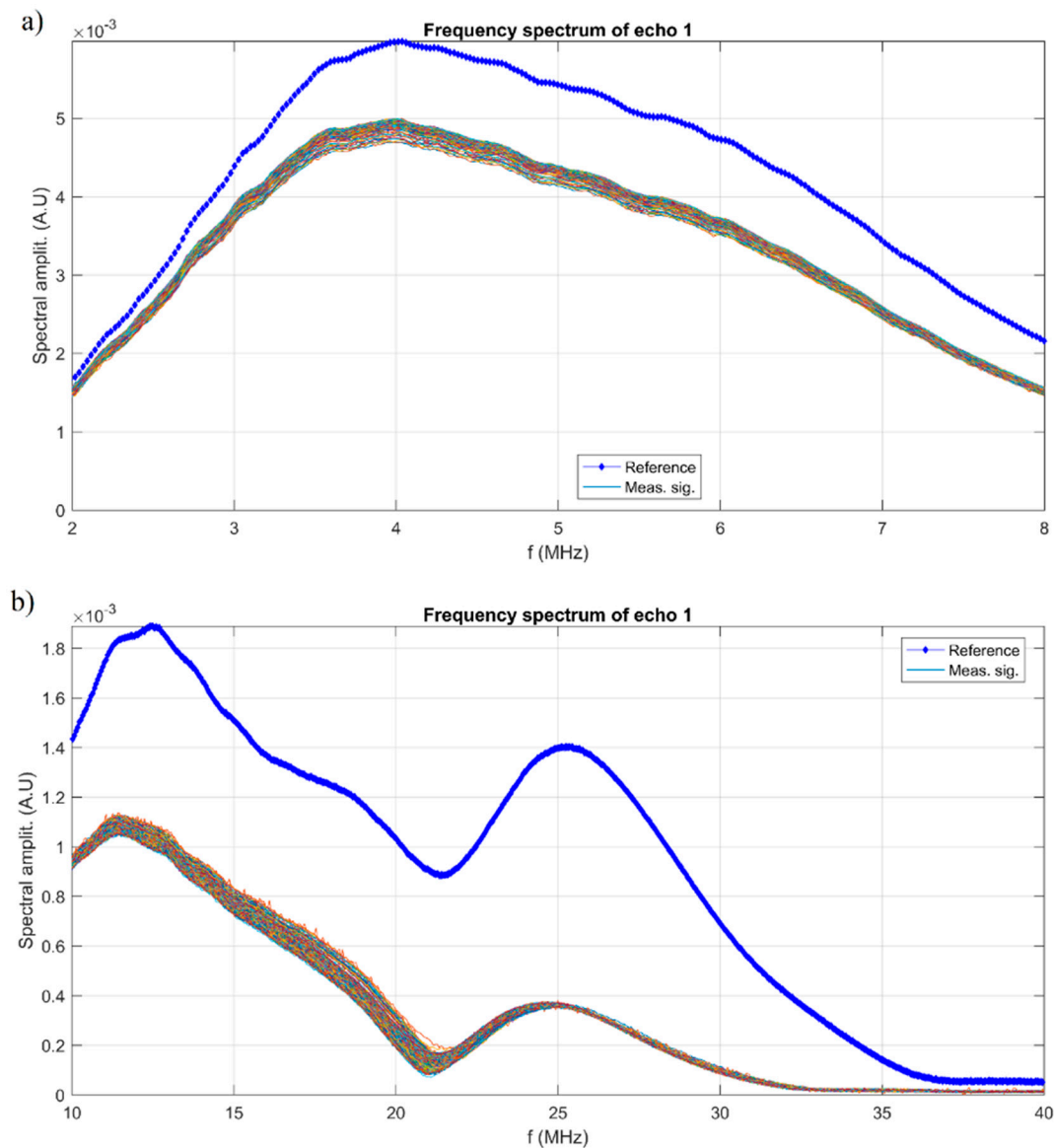


**Figure 1.** Frequency spectrum of the first transmitted echo at 5 MHz (a) and 25 MHz (b) central frequency for the AgZnHApCs suspension.

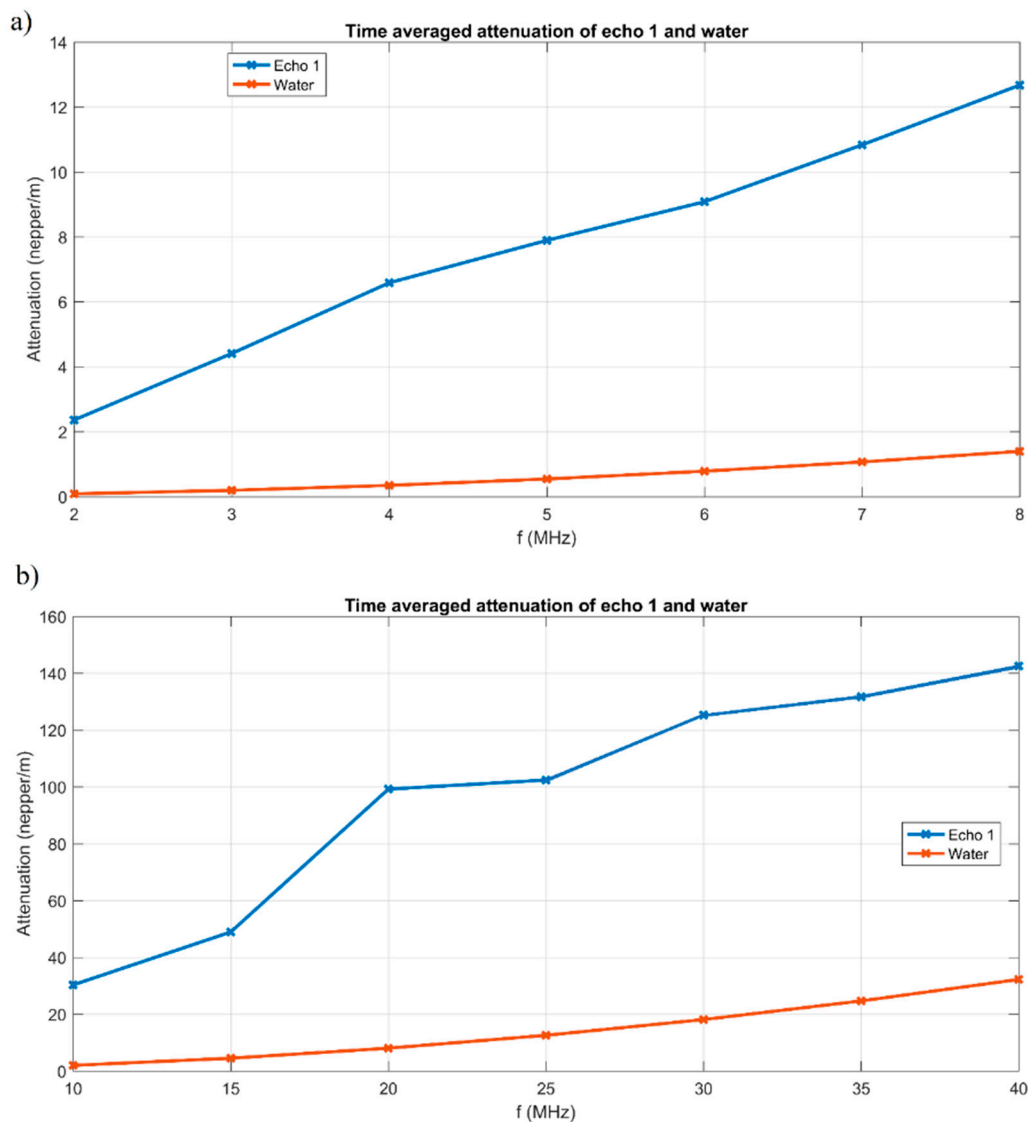


**Figure 2.** Attenuation vs. frequency for the first transmitted echo at 5 MHz (a) and 25 MHz (b) central frequency for the AgZnHApCs suspension.

The XRD studies were conducted in order to evaluate the crystalline structure of biocomposites suspension and coatings based on silver and zinc doped hydroxyapatite in chitosan matrix prepared from the sol-gel process (Figure 3). XRD patterns on the powder obtained from the AgZnHApCs gel are shown in Figure 3a. XRD pattern of the AgZnHApCs coatings (Figure 3b) and chitosan (Figure 3c) and the standard pattern of the HAp (JCPDS card No.09-0432) and chitosan PDF-00-054-1952 are also presented.

The XRD patterns of AgZnHApCs powder (Figure 3a) and coatings (Figure 3b) revealed the main diffraction peaks identified at different  $2\theta$  values that were assigned to the position of the planes of pure hexagonal HAp at (002), (211), (112), (300), (202), (310), (222), (213), (004), (323), in agreement with JCPDScardNo.09-0432 [36]. In order to calculate the average size all, the peaks of the XRD pattern were taken into account. The mean crystallite size was calculated using Scherrer's formula

$$D = 0.9\lambda/\beta \times \cos \theta. \quad (1)$$

In the Scherrer's formula,  $D$  represents the average crystallite size,  $\beta$  the peak broadening of the diffraction line measured at half of its maximum intensity,  $\lambda$  the wavelength of X-rays, and  $\theta$  the

Bragg's diffraction angle. The mean crystallite size of AgZnHApCs powders (Figure 3a) was found to be  $18 \pm 2$  nm, while the mean crystallite size of AgZnHApCs coatings (Figure 3b) was found to be  $15 \pm 3$  nm.

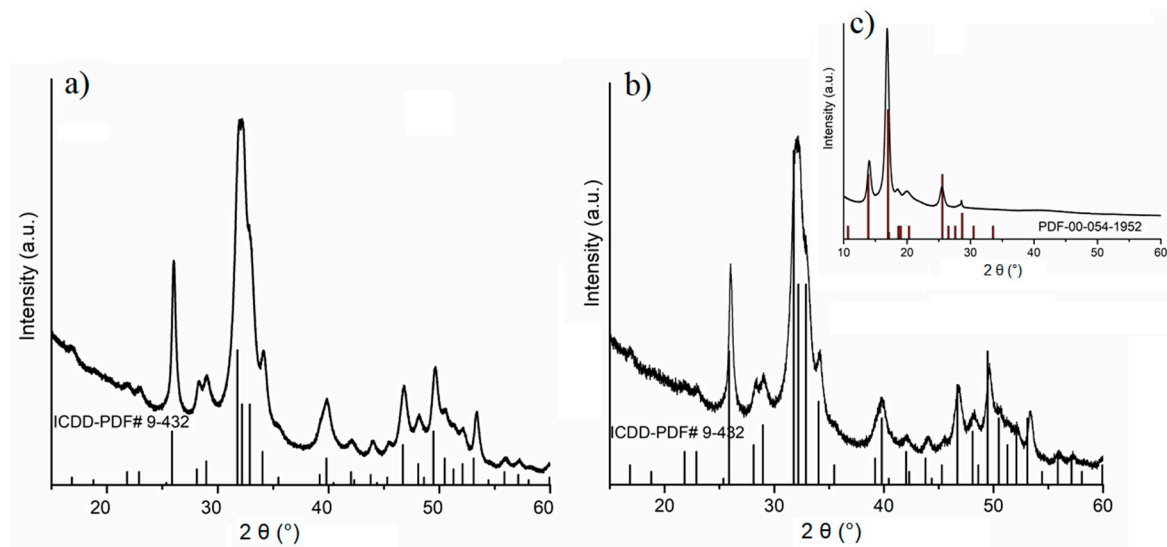


**Figure 3.** XRD pattern of the AgZnHApCs powder (a), AgZnHApCs coatings (b) and Chitosan (c) and the standard pattern of the HAp (JCPDS card No.09-0432) and Chitosan PDF-00-054-1952.

FTIR analysis revealed the presence of chitosan on the AgZnHApCs suspension and coating. FTIR spectra of AgZnHApCs suspension, AgZnHApCs coating and Cs recorded over the range of  $400\text{--}4000\text{ cm}^{-1}$  were presented in Figure 4. The spectra of AgZnHApCs suspension and AgZnHApCs coating exhibit characteristic vibrational modes of HAp and chitosan, proving that the AgZnHAp nanoparticles were successfully coated with chitosan. The two samples spectra (AgZnHApCs suspension and AgZnHApCs coating) showed specific phosphate vibrational modes ( $\nu_4$ ) at  $571$ ,  $604$  and  $636\text{ cm}^{-1}$ . The peaks at  $571$  and  $604\text{ cm}^{-1}$  correspond to a triply degenerated bending mode of the O–P–O band [34]. The peak at  $636\text{ cm}^{-1}$  was also assigned to the hydroxyl group deformation mode [36]. According to previous studies [36,37], the peak at  $632\text{ cm}^{-1}$  is considered to be overlapped with an asymmetric P–O stretching vibration of  $\text{PO}_4^{3-}$ . The bands at around  $1088$  and  $1047\text{ cm}^{-1}$  in the region  $900\text{--}1200\text{ cm}^{-1}$  were attributed to the C–O–P stretching and phosphorylated hydroxyl group, while the peaks at around  $473$  and  $998\text{ cm}^{-1}$  may be assigned for P–OH groups. The bands assigned to P–O, P=O stretching of phosphate group can be observed at around  $1100$  to  $1250\text{ cm}^{-1}$  in the region  $900\text{--}1200\text{ cm}^{-1}$ . According to previous studies on the interactions of calcium phosphates with chitosan [38,39], the peaks in the region  $1300\text{--}1450\text{ cm}^{-1}$  can be attributed to a combination of CN–NH,  $\text{CH}_2\text{--OH}$  and  $\text{CH}_3$  bands. The band from  $1422\text{ cm}^{-1}$  can be assigned to the bending CH vibrations, while the peak from  $1076\text{ cm}^{-1}$  in the region  $1008\text{--}1150\text{ cm}^{-1}$  can be assigned to groups C–O–C. The absorption bands at  $1315$ ,  $1372$  and  $1407\text{ cm}^{-1}$  were assigned to the carbonate bands of acetic acid which were not observed in the spectra. On the other hand, the presence of carbonate bands of acetic acid should be avoided for biocompatible applications [38,39]. The peak at  $1642\text{ cm}^{-1}$  can be assigned to the N–H from chitosan. The AgZnHApCs in suspension and AgZnHAp coating showed typical bands characteristic to HAp and chitosan, as can be exhibited in Figure 4b,c.

The morphology of the AgZnHApCs coating's surface was studied by AFM analysis. The 2D AFM topography of the AgZnHApCs coating's surface is presented in Figure 5a and the 3D representation of the surface morphology of AgZnHApCs coating is depicted in Figure 5b. The 2D AFM micrograph and the 3D representation of the AgZnHApCs coating's surface highlighted that the AgZnHApCs coating's surface exhibited the morphology of a uniformly deposited layer. In addition, the AFM topography also suggested that the surface of the coating does not present any cracks or fissures and is composed

of equally distributed nanoaggregates. The AFM results emphasized that the surface topography of the AgZnHApCs coating was homogenous, having a roughness ( $R_{RMS}$ ) value of 43.1125 nm.

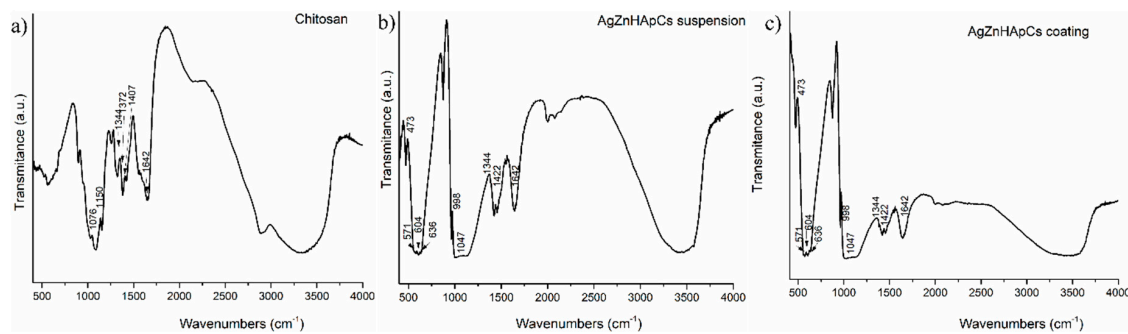


**Figure 4.** FTIR spectra of chitosan (a), AgZnHApCs suspension (b) and AgZnHApCs coating (c).

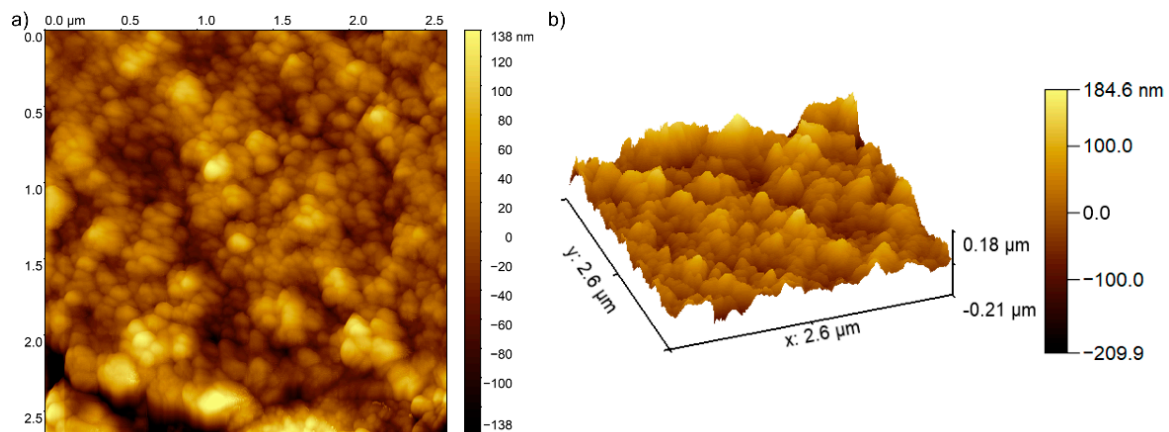


**Figure 5.** Representation of the atomic force microscopy (AFM) topography image of the AgZnHApCs coating's surface (a) and 3D representation of the surface topography of AgZnHApCs coatings (b).

Moreover, the surface morphology of the AgZnHApCs coating was also studied by optical and metallographic microscopy. The 2D images with the optical and metallographic microscope were acquired using the 10× objective. The results are presented in Figures 6a and 7a. The optical images of the surface of the AgZnHApCs coating emphasized that the coatings deposited on glass substrate are homogenous and uniform, having no visible discontinuities, fissures or irregularities. In addition, the 3D representation of the optical image of AgZnHApCs coating's surface obtained using ImageJ software [32] is depicted in Figure 6b.

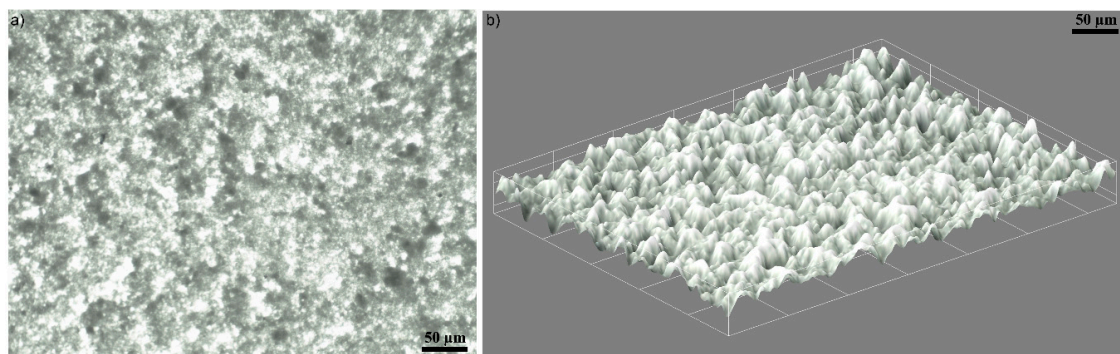


**Figure 6.** Optical microscopy image (10× magnification) of the AgZnHApCs coating's surface (a) and 3D representation of the surface of the AgZnHApCs coating (b).

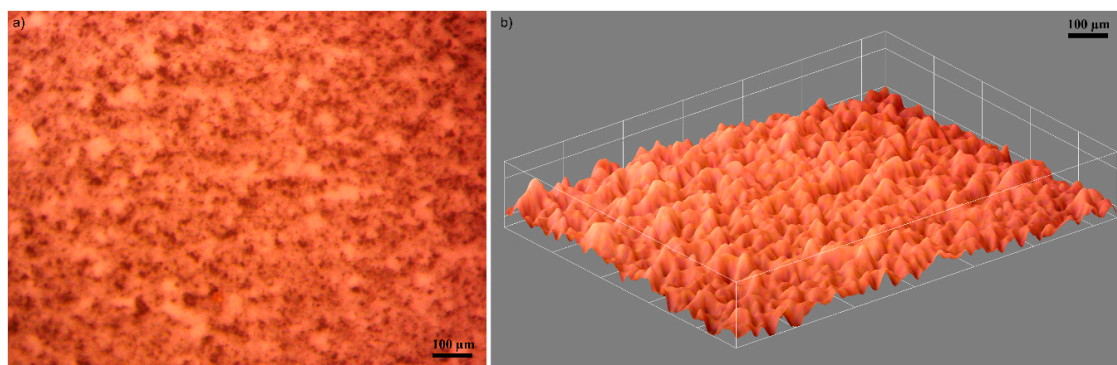


**Figure 7.** Metallographic microscopy image (10× magnification) of the AgZnHApCs coating's surface (a) and 3D representation of the surface of the AgZnHApCs coating (b).

Complementary information regarding the morphology of the AgZnHApCs coating deposited on glass substrate was also obtained using a metallographic microscope. The 2D image of the AgZnHApCs coating's surface obtained with the 10x objective of the metallographic microscope is depicted in Figure 7a. Similar to the optical microscopy studies, the metallographic investigations highlighted that the surface of AgZnHApCs coating has an evenly homogenous morphology and do not exhibit any fissures or cracks. Moreover, the 3D representation of the metallographic microscope 2D image of the AgZnHApCs coating's surface depicted in Figure 7b confirmed the results of the optical microscopy studies, and revealed that the AgZnHApCs coatings are continuous, with no cracks or fissures.

The *in vitro* biocompatibility of the AgZnHApCs suspensions and coatings was assessed using human fetal osteoblasts (hFOB 1.19) cells. For this purpose, the suspension and coatings were incubated with the hFOB 1.19 cell suspension for different time intervals (1, 7 and 14 days) and their viability was measured by MTT assay. The MTT results of the hFOB 1.19 cell viability are depicted in Figure 8. The experiments were repeated four times and the data were presented as mean  $\pm$  SD. Furthermore, a *t*-test: paired two sample for means was used to perform the statistical analysis, and all the *p* calculated values were  $p < 0.05$ . The results revealed that both investigated samples presented a cell viability above 85% for all tested time intervals. Moreover, the results also highlighted that there was no significant difference between the samples in the form of suspension and coatings. However, a slight increase in cell viability was observed in the case of AgZnHApCs suspensions compared to the AgZnHApCs coatings for all incubation periods. Moreover, the data also suggested that the cell viability increased with the increase of the incubation time. The results showed that both samples present very good biocompatible and bioactive properties. The results are in agreement with previous studies performed to date, regarding the hydroxyapatite properties of facilitating the attachment and growth of osteoblast cells due to its high hydrophilic property [40,41].

The morphology of the hFOB 1.19 cells incubated for 1, 7 and 14 days with the AgZnHApCs suspensions and coatings was also assessed using an inverted microscope. The morphology of the hFOB 1.19 cells treated with AgZnHApCs suspensions and coatings after 1, 7 and 14 days of incubation are depicted in Figure 9. The images of the hFOB 1.19 cells incubated with AgZnHApCs suspensions and coatings at different time intervals show the normal morphology of the hFOB 1.19 cells and revealed that the suspensions and coatings did not induce any significant changes in the hFOB 1.19 cells. These results are in agreement with the results of the quantitative MTT *in vitro* assay, and highlighted that both AgZnHApCs suspensions and coatings have a good biocompatibility and are suitable for being used in biomedical applications.

The antimicrobial activities of the AgZnHApCs suspensions and coatings were also assessed using reference gram positive, gram negative and fungal microbial strains. The antimicrobial properties of AgZnHApCs suspensions and coatings were assessed at three different time intervals of incubation (24, 48 and 72 h) against *S. aureus* ATCC 25923, *E. coli* ATCC 25922, and *C. albicans* ATCC 9002, by assessing the colony forming units (CFU) inhibition for each tested microbial strain. The results of

the antimicrobial assay are presented in Figure 10. The antimicrobial assays were repeated four times and the data were represented as mean  $\pm$  SD. A free microbial suspension was also assessed and used as positive control (C+) for all tested time intervals. The statistical analysis was done using the ANOVA single factor algorithm and the calculated  $p$ -values were less than 0.0001 [42,43]. The data revealed that the AgZnHApCs suspensions and coatings exhibited strong antimicrobial activity against all the tested strains, even after 24 h of incubation. The CFU values were significantly reduced after 24 h of incubation with the suspensions and coatings. The results of the antimicrobial assays also suggested that the CFU inhibition was significant for all tested samples and that was correlated with the incubation time. Moreover, the results revealed that the antimicrobial activity of the suspensions was greater than that of the coatings for all tested microbial strains at all tested time intervals. In addition, a fungicidal effect was noticed in the case of AgZnHApCs suspensions after 48 h and 72 h of exposure, and in the case of AgZnHApCs coatings after 72 h of incubation. The results revealed by the antimicrobial assays are in agreement with previously reported data from the literature regarding the antimicrobial properties of silver and zinc ions [5–8,44–53]. Moreover, the results are in accordance with literature data reported on the potential antimicrobial properties of materials and composite layers based on hydroxyapatite enhanced with metal ions in polymeric matrix which possess antimicrobial activity. Furthermore, the statistical analysis emphasized that the data supports that both AgZnHApCs suspensions and coatings present antimicrobial activities on the tested microbial strains and that the AgZnHApCs suspensions exhibited a greater antimicrobial activity than AgZnHApCs coatings.

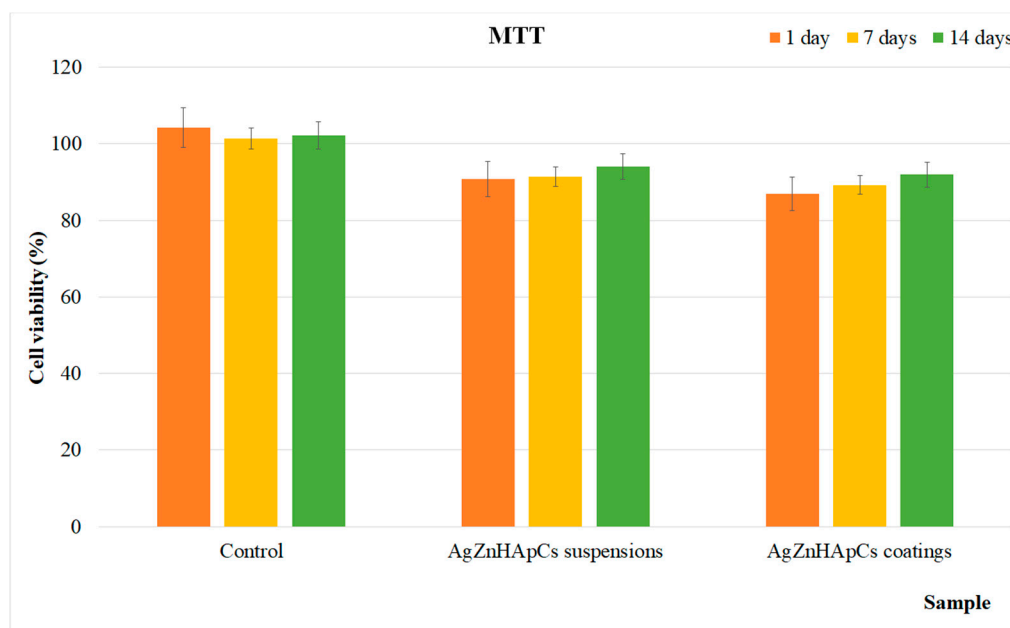


**Figure 8.** MTT assay for the viability of hFOB 1.19 cells incubated on AgZnHApCs suspensions and coatings for 1 day, 7 days and 14 days. The results are presented as means  $\pm$  standard error of the mean of four independent experiments. The data were statistically analyzed by using a  $t$ -Test: Paired Two Sample for Means and  $p$  values,  $p \leq 0.05$ , were accepted as statistically significant.

Despite the reported studies regarding the antimicrobial activity of metallic ions such as silver and zinc, data regarding the synergies formed between the chemical components of composites based on hydroxyapatite and metal ions in polymeric matrix are still limited. In this case, the antimicrobial properties of the AgZnHApCs suspensions and coatings could be attributed both to their constituent elements and to the synergies that appear in the composite. Therefore, the antimicrobial properties obtained in our studies could be attributed both to the presence of the silver and zinc ions, as well as to the synergy that formed between the zinc, silver and chitosan components with the hydroxyapatite structure and with the glass substrate in the case of AgZnHApCs coatings. Moreover, our results also

suggested that the nature of the sample, either suspension or coating, has an important role in their biological activity. Both the cytotoxic assay and the antimicrobial assay revealed that the biological properties of the AgZnHApCs suspensions were better than the ones of the AgZnHApCs coatings.

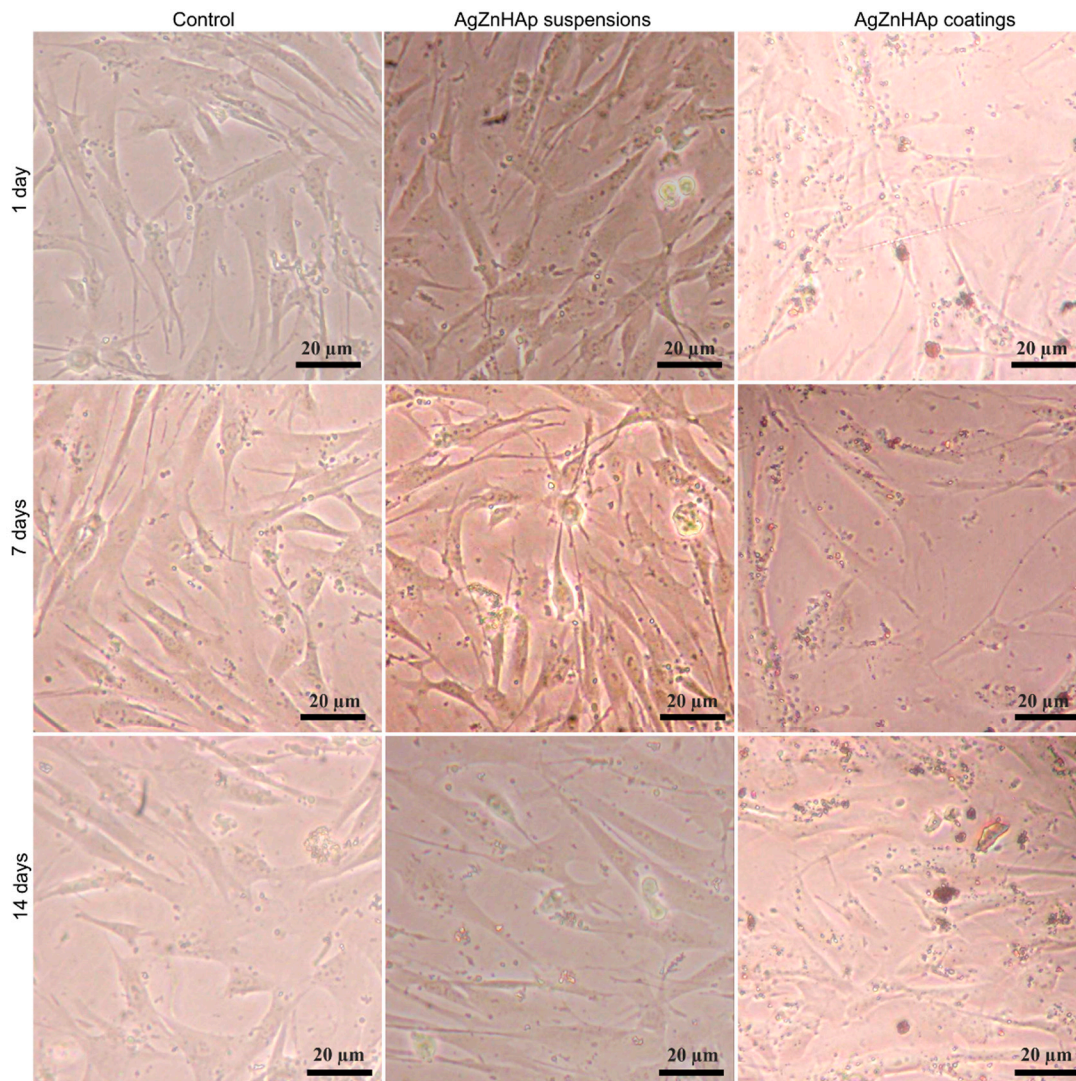


**Figure 9.** The morphology of the hFOB 1.19 cells incubated with AgZnHApCs suspensions and coatings after 1, 7 and 14 days.

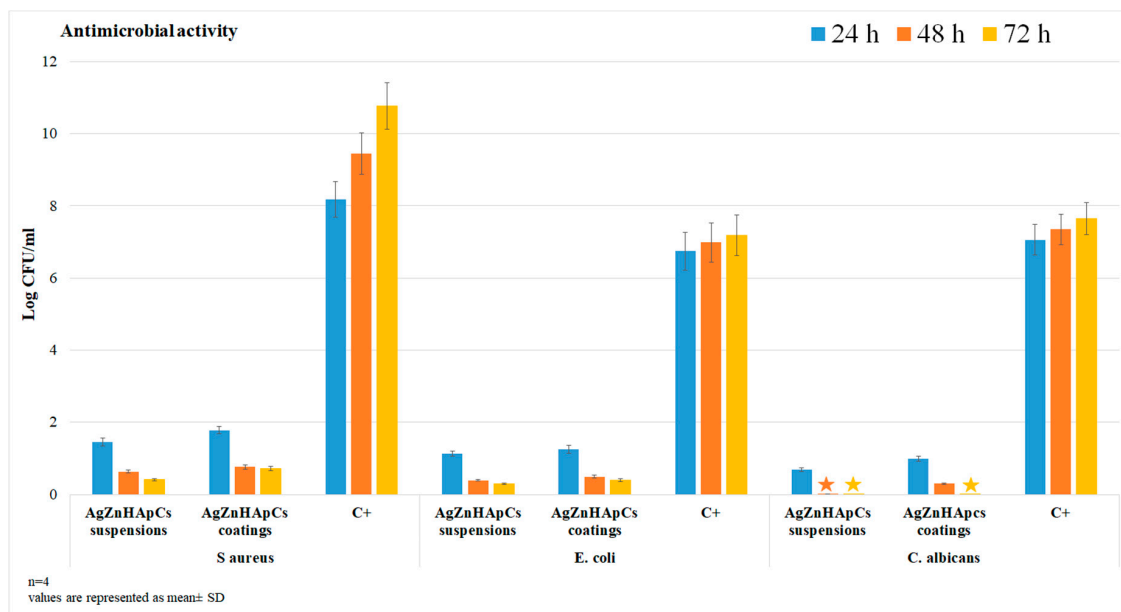


**Figure 10.** The graphical representation of the Log colony forming units (CFU)/mL of *S. aureus* ATCC 25923, *E. coli* ATCC 25922, and *C. albicans* ATCC 9002 for different incubation times with AgZnHApCs suspensions and coatings. The results are presented as means  $\pm$  standard error of the mean of 4 independent experiments. The data was statistically analyzed by ANOVA Single Factor algorithm and the calculated  $p$ -values were less than 0.0001.

#### 4. Conclusions

A novel AgZnHApCs composite suspension with superior biocompatibility and significant antibacterial activity has been synthesized by an adapted coprecipitation method, in order to prepare the AgZnHApCs composite coatings by dip coating method. The FTIR and XRD evaluation showed the bonding interaction between silver and zinc doped hydroxyapatite and chitosan. The homogeneous dispersion and the stability of nanoparticles in the chitosan matrix have been evaluated. The morphology and homogeneity of the surface coatings were investigated by optical spectroscopy, AFM and metallographic examination and XPS. The use of chitosan provides a significant increasing of dispersion of nanoparticles. FTIR analysis revealed the chemical bond interaction between Ca ions and  $-OH$  groups of HAp and a combination of  $CN-NH$ ,  $CH_2-OH$  and  $CH_3$  bands assigned of chitosan. MTT test confirms that the AgZnHApCs suspension and coatings composite are cytocompatible. hFOB 1.19 cell culture study proves that the AgZnHApCs suspension and coatings composite do not influence cell morphology and proliferation. The antimicrobial assays conducted against *Staphylococcus aureus* ATCC 25923, *Escherichia coli* ATCC 25922, and *Candida albicans* ATCC 90029 microbial strains revealed that both the AgZnHApCs composite suspension and coatings exhibited great antimicrobial properties. In addition, the results have emphasized that the suspension were more effective against the tested microbial strains. The results of our studies suggest that the novel developed AgZnHApCs nanocomposite coatings can be used in different fields, such as the surface modification of bone implants, and ameliorate the osteoconductivity of bone regeneration.

**Author Contributions:** Conceptualization, D.P. and M.V.P.; methodology, D.P.; software, M.V.P.; validation, D.P., S.L.I. and M.V.P.; formal analysis, D.P.; investigation, S.L.I.; resources, D.P.; data curation, D.P.; writing—original draft preparation, D.P., S.L.I. and M.V.P.; writing—review and editing, D.P., S.L.I. and M.V.P.; visualization, D.P., S.L.I. and M.V.P.; supervision, D.P.; project administration, M.V.P.; funding acquisition, M.V.P. All authors have read and agreed to the published version of the manuscript.

**Funding:** This research was funded by Romanian Ministry of Research and Innovation with the grant number PN-III-P1-1.2-PCCDI-2017-0629/contract No. 43PCCDI/2018 and Scientific Research Contract

Nr.1/4.06.2020] and “The APC was funded by [Romanian Ministry of Research and Innovation] project number PN-III-P1-1.2-PCCDI-2017-0629/contract No. 43PCCDI/2018.”

**Acknowledgments:** We would like to thank M.L. Badea for her help with the acquisition of the biological assays data.

**Conflicts of Interest:** The authors declare no conflict of interest.

## References

1. Mocanu, A.; Furtos, G.; Rapuntean, S.; Horowitz, O.; Flore, C.; Garbo, C.; Danisteanu, A.; Rapuntean, G.; Prejmerean, C.; Tomoaia-Cotisel, M. Synthesis; characterization and antimicrobial effects of composites based on multi-substituted hydroxyapatite and silver nanoparticles. *Appl. Surf. Sci.* **2014**, *298*, 225–235. [[CrossRef](#)]
2. Radovanovic, Z.; Jokic, B.; Veljovic, D.; Dimitrijevic, S.; Kojic, V.; Petrovic, R.; Janackovic, D. Antimicrobial activity and biocompatibility of Ag<sup>+</sup>- and Cu<sup>2+</sup>-doped biphasic hydroxyapatite/ $\alpha$ -tricalcium phosphate obtained from hydrothermally synthesized Ag<sup>+</sup>- and Cu<sup>2+</sup>-doped hydroxyapatite. *Appl. Surf. Sci.* **2014**, *307*, 513–519. [[CrossRef](#)]
3. Shanmugam, S.; Gopal, B. Antimicrobial and cytotoxicity evaluation of aliovalent substituted hydroxyapatite. *Appl. Surf. Sci.* **2014**, *303*, 277–281. [[CrossRef](#)]
4. Van Hengel, I.A.J.; Putra, N.E.; Tierolf, M.W.A.M.; Minneboo, M.; Fluit, A.C.; Fratila-Apachitei, L.E.; Apachitei, L.; Zadpoor, A.A. Biofunctionalization of selective laser melted porous titanium using silver and zinc nanoparticles to prevent infections by antibiotic-resistant bacteria. *Acta Biomater.* **2020**, *107*, 325–337. [[CrossRef](#)] [[PubMed](#)]
5. Ohtsu, N.; Kakuchi, Y.; Ohtsuki, T. Antibacterial effect of zinc oxide/hydroxyapatite coatings prepared by chemical solution deposition. *Appl. Surf. Sci.* **2018**, *445*, 596–600. [[CrossRef](#)]
6. Predoi, D.; Iconaru, S.L.; Predoi, M.V. Dextran-coated zinc-doped hydroxyapatite for biomedical applications. *Polymers* **2019**, *11*, 886. [[CrossRef](#)]
7. Predoi, D.; Iconaru, S.L.; Predoi, M.V. Bioceramic layers with antifungal properties. *Coatings* **2018**, *8*, 276. [[CrossRef](#)]
8. Predoi, D.; Iconaru, S.L.; Deniaud, A.; Chevallet, M.; Michaud-Soret, I.; Buton, N.; Prodan, A.M. Textural, structural and biological evaluation of hydroxyapatite doped with zinc at low concentrations. *Materials* **2017**, *10*, 229. [[CrossRef](#)]
9. Iqbal, N.; Kadir, M.R.A.; Mahmood, N.H.; Salim, N.; Froemming, G.R.A.; Balaji, H.R.; Kamarul, T. Characterization, antibacterial and in vitro compatibility of zinc–silver doped hydroxyapatite nanoparticles prepared through microwave synthesis. *Ceram. Int.* **2014**, *40*, 4507–4513. [[CrossRef](#)]
10. Chen, W.; Oh, S.; Ong, A.P.; Oh, N.; Liu, Y.; Courtney, H.S.; Appleford, M.; Ong, J.L. Antibacterial and osteogenic properties of silver-containing hydroxyapatite coatings produced using a sol–gel process. *J. Biomed. Mater. Res. A* **2007**, *82*, 899–906. [[CrossRef](#)]
11. Helen, S.; Ruban Kumar, A. Study of structural, mechanical and dielectrical properties of ions doped apatite for antibacterial activity. *Mater. Chem. Phys.* **2019**, *237*, 121867. [[CrossRef](#)]
12. Ciobanu, C.S.; Iconaru, S.L.; Chifiriuc, M.C.; Costescu, A.; Le Coustumer, P.; Predoi, D. Synthesis and antimicrobial activity of silver-doped hydroxyapatite nanoparticles. *Biomed. Res. Int.* **2013**, *2013*, 916218. [[CrossRef](#)] [[PubMed](#)]
13. Ciobanu, C.S.; Massuyeau, F.; Constantin, L.V.; Predoi, D. Structural and physical properties of antibacterial Ag-doped nano-hydroxyapatite synthesized at 100 °C. *Nanoscale Res. Lett.* **2011**, *6*, 613. [[CrossRef](#)] [[PubMed](#)]
14. Costescu, A.; Ciobanu, C.S.; Iconaru, S.L.; Ghita, R.V.; Chifiriuc, C.M.; Marutescu, L.G.; Predoi, D. Fabrication, characterization, and antimicrobial activity, evaluation of low silver concentrations in silver-doped hydroxyapatite nanoparticles. *J. Nanomater.* **2013**, *2013*, 194854. [[CrossRef](#)]
15. Furko, M.; Havasi, V.; Kónya, Z.; Grünwald, A.; Detsch, R.; Boccaccini, A.R.; Balázs, C. Development and characterization of multi-element doped hydroxyapatite bioceramic coatings on metallic implants for orthopedic applications. *Boletín de la Sociedad Española de Cerámica y Vidrio* **2018**, *57*, 55–65. [[CrossRef](#)]
16. Chou, Y.J.; Ningsih, H.S.; Shih, S.-J. Preparation, characterization and investigation of antibacterial silver-zinc co-doped  $\beta$ -tricalcium phosphate by spray pyrolysis. *Ceram. Int.* **2020**, *46*, 16708–16715. [[CrossRef](#)]
17. Ofudje, E.A.; Adeogun, A.I.; Idowu, M.A.; Kareem, S.O. Synthesis and characterization of Zn-doped hydroxyapatite: Scaffold application, antibacterial and bioactivity studies. *Heliyon* **2019**, *5*, e01716. [[CrossRef](#)]

18. Chen, X.; Tang, Q.-L.; Zhu, Y.-J.; Zhu, C.-L.; Feng, X.-P. Synthesis and antibacterial property of zinc loaded hydroxyapatite nanorods. *Mater. Lett.* **2012**, *89*, 233–235. [[CrossRef](#)]
19. Xie, Y.; He, Y.; Irwin, P.L.; Jin, T.; Shi, X. Antibacterial activity and mechanism of action of zinc oxide nanoparticles against *Campylobacter jejuni*. *Appl. Environ. Microbiol.* **2011**, *77*, 2325–2331. [[CrossRef](#)]
20. Mirhashemi, A.; Bahador, A.; Kassae, M.; Daryakenari, G.; Ahmad-Akhoundi, M.; Sodagar, A. Antimicrobial Effect of nano-zinc oxide and nano-chitosan particles in dental composite used in orthodontics. *J. Med. Bacteriol.* **2013**, *2*, 1–10.
21. Haldorai, Y.; Shim, J.-J. Chitosan-zinc oxide hybrid composite for enhanced dye degradation and antibacterial activity. *Compos. Interfaces* **2013**, *20*, 365–377. [[CrossRef](#)]
22. Wu, S.; Ma, S.; Zhang, C.; Cao, G.; Wu, D.; Gao, C.; Lakshmanan, S. Cryogel biocomposite containing chitosan-gelatin/cerium–zinc doped hydroxyapatite for bone tissue engineering. *Saudi J. Biol. Sci.* **2020**, *27*, 2638–2644. [[CrossRef](#)]
23. Ciobanu, C.S.; Iconaru, S.L.; Massuyeau, F.; Constantin, L.V.; Costescu, A.; Predoi, D. Synthesis, structure, and luminescent properties of europium-doped hydroxyapatite nanocrystalline powders. *J. Nanomater.* **2012**, *2012*, 942801. [[CrossRef](#)]
24. Iconaru, S.L.; Motelica-Heino, M.; Guegan, R.; Predoi, M.V.; Prodan, A.M.; Predoi, D. Removal of zinc ions using hydroxyapatite and study of ultrasound behavior of aqueous media. *Materials* **2018**, *11*, 1350. [[CrossRef](#)]
25. Ciobanu, C.S.; Iconaru, S.L.; Popa, C.L.; Motelica-Heino, M.; Predoi, D. Evaluation of samarium doped hydroxyapatite, ceramics for medical application: Antimicrobial activity. *J. Nanomater.* **2015**, *2015*, 849216. [[CrossRef](#)]
26. Rodriguez, L.; Matoušek, J. Preparation of TiO<sub>2</sub> sol-gel layers on glass. *Ceram. Silik.* **2003**, *47*, 28–31.
27. Predoi, D.; Iconaru, S.L.; Predoi, M.V.; Motelica-Heino, M.; Guegan, R.; Buton, N. Evaluation of antibacterial activity of zinc-doped hydroxyapatite colloids and dispersion stability using ultrasounds. *Nanomaterials* **2019**, *9*, 515. [[CrossRef](#)]
28. Predoi, D.; Predoi, M.V.; Iconaru, S.L.; Ech Cherif El Kettani, M.; Leduc, D.; Prodan, A.M. Ultrasonic Measurements on  $\beta$  Cyclodextrin/Hydroxyapatite Composites for Potential Water Depollution. *Materials* **2017**, *10*, 681. [[CrossRef](#)]
29. Predoi, D.; Iconaru, S.L.; Predoi, M.V.; Motelica-Heino, M. Removal and oxidation of As(III) from water using iron oxide coated CTAB as adsorbent. *Polymers* **2020**, *12*, 1687. [[CrossRef](#)]
30. Yamaguchi, M. Role of zinc in bone formation and bone resorption. *J. Trace Elem. Exp. Med.* **1998**, *11*, 119–135. [[CrossRef](#)]
31. Predoi, D.; Iconaru, S.L.; Predoi, M.V.; Motelica-Heino, M.; Buton, N.; Megier, C. Obtaining and characterizing thin layers of magnesium doped hydroxyapatite by dip coating procedure. *Coatings* **2020**, *10*, 510. [[CrossRef](#)]
32. Gwyddion. Available online: <http://gwyddion.net/> (accessed on 20 January 2020).
33. ImageJ. Available online: <http://imagej.nih.gov/ij> (accessed on 10 January 2018).
34. Predoi, D.; Vatasescu-Balcan, R.A. Osteoblast interaction with iron oxide nanoparticles coated with dextrin in cell culture. *J. Optoelectron. Adv. Mat.* **2008**, *10*, 152–157.
35. Predoi, D.; Iconaru, S.L.; Buton, N.; Badea, M.L.; Marutescu, L. Antimicrobial activity of new materials based on lavender and basil essential oils and hydroxyapatite. *Nanomaterials* **2018**, *8*, 291. [[CrossRef](#)] [[PubMed](#)]
36. Ciobanu, C.S.; Iconaru, S.L.; Le Coustumer, P.; Predoi, D. Vibrational investigations of silver-doped hydroxyapatite with antibacterial properties. *J. Spectrosc.* **2013**, *2013*, 1–5. [[CrossRef](#)]
37. Negrila, C.C.; Predoi, M.V.; Iconaru, S.L.; Predoi, D. Development of zinc-doped hydroxyapatite by sol-gel method for medical applications. *Molecules* **2018**, *23*, 2986. [[CrossRef](#)]
38. Ruphuy, G.; Saralegi, A.; Lopes, J.C.; Dias, M.M.; Barreiro, M.F. Spray drying as a viable process to produce nano-hydroxyapatite/chitosan (n-HAp/CS) hybrid microparticles mimicking bone composition. *Adv. Powder Technol.* **2016**, *27*, 575–583. [[CrossRef](#)]
39. Fadeeva, I.V.; Barinov, S.M.; Fedotov, A.Y.; Komlev, V.S. Interactions of calcium phosphates with chitosan. *Dokl. Chem.* **2011**, *441*, 387–390. [[CrossRef](#)]
40. Silverstein, R.M.; Webster, F.X.; Kiemle, D.; Bryce, D.L. *Spectrometric Identification of Organic Compounds*, 8th ed.; John Wiley & Sons: Hoboken, NJ, USA, 2014.

41. Thian, E.S.; Ahmad, Z.; Huang, J.; Edirisinghe, M.J.; Jayasinghe, S.N.; Ireland, D.C.; Brooks, R.A.; Rushton, N.; Bonfield, W.; Best, S.M. The role of surface wettability and surface charge of electrosprayed nanoapatites on the behaviour of osteoblasts. *Acta Biomater.* **2010**, *6*, 750–755. [[CrossRef](#)]
42. Cabral, D.J.; Penumutthu, S.; Norris, C.; Morones-Ramirez, J.R.; Belenky, P. Microbial competition between *Escherichia coli* and *Candida albicans* reveals a soluble fungicidal factor. *Microb. Cell* **2018**, *5*, 249–255. [[CrossRef](#)]
43. Lorowitz, W.; Saxton, E.; Sondossi, M.; Nakaoka, K. Integrating statistics with a microbiology laboratory activity. *J. Microbiol. Biol. Educ.* **2005**, *6*, 14–19. [[CrossRef](#)]
44. Kilpadi, K.L.; Chang, P.-L.; Bellis, S.L. Hydroxylapatite binds more serum proteins, purified integrins, and osteoblast precursor cells than titanium or steel. *J. Biomed. Mater. Res.* **2001**, *57*, 258–267. [[CrossRef](#)]
45. Zhang, D.; Lepparanta, O.; Munukka, E.; Ylanen, H.; Viljanen, M.K.; Eerola, E.; Hupa, M.; Hupa, L. Antibacterial effects and dissolution behavior of six bioactive glasses. *J. Biomed. Mater. Res. A* **2010**, *93*, 475–483. [[CrossRef](#)] [[PubMed](#)]
46. Gopi, D.; Sathishkumar, S.; Karthika, A.; Kavitha, L. Development of Ce<sup>3+</sup>/Eu<sup>3+</sup> Dual-Substituted Hydroxyapatite Coating on Surgical Grade Stainless Steel for Improved Antimicrobial and Bioactive Properties. *Ind. Eng. Chem. Res.* **2014**, *53*, 20145–20153. [[CrossRef](#)]
47. Kolmas, J.; Groszyk, E.; Kwiatkowska-Różycka, D. Substituted Hydroxyapatites with Antibacterial Properties. *BioMed Res. Int.* **2014**, *2014*, 1–15. [[CrossRef](#)] [[PubMed](#)]
48. Wang, Y.Z.; Xue, X.X.; Yang, H. Preparation and characterization of zinc and cerium co-doped titania nano-materials with antibacterial activity. *J. Inorg. Mater.* **2013**, *28*, 117–122. [[CrossRef](#)]
49. Bhadra, P.; Mitra, M.K.; Das, G.C.; De, R.; Mukherjee, S. Interaction of chitosan capped ZnO nanorods with *Escherichia coli*. *Mater. Sci. Eng. C* **2011**, *31*, 929–937. [[CrossRef](#)]
50. Mujeeb Rahman, P.; Abdul Mujeeb, V.M.; Muraleedharan, K.; Steni, K.T. Chitosan/nano ZnO composite films: Enhanced mechanical, antimicrobial and dielectric properties. *Arab. J. Chem.* **2018**, *11*, 120–127. [[CrossRef](#)]
51. Goy, R.C.; De Britto, D.; Assis, O.B.G. A review of the antimicrobial activity of chitosan. *Polímeros* **2009**, *19*, 241–247. [[CrossRef](#)]
52. Zheng, L.-Y.; Zhu, J.-F. Study on antimicrobial activity of chitosan with different molecular weights. *Carbohydr. Polym.* **2003**, *54*, 527–530. [[CrossRef](#)]
53. Devlieghere, F.; Vermeulen, A.; Debevere, J. Chitosan: Antimicrobial activity, interactions with food components and applicability as a coating on fruit and vegetables. *Food Microbiol.* **2004**, *21*, 703–714. [[CrossRef](#)]

